Available online at www.sciencedirect.com

ScienceDirect

Procedia Manufacturing 48 (2020) 797–806

Procedia MANUFACTURING

www.elsevier.com/locate/procedia

48th SME North American Manufacturing Research Conference, NAMRC 48 (Cancelled due to COVID-19)

Hydrothermal Assisted Transient Jet Fusion of Ceramics: A Test Case Using Bentonite Clay

Levi Kirby[a], Fan Fei[a], Chao Wang[a], Xuan Song[a,b,*]

[a]*Department of Industrial and Systems Engineering, The University of Iowa, Iowa City, IA 52242, United States*
[b]*Iowa Technology Institute, The University of Iowa, Iowa City, IA 52242, United States*

* Corresponding author. Tel.: +1-319-335-5680; fax: +1-319-335-6086. *E-mail address:* xuan-song@uiowa.edu

Abstract

This paper presents a new additive manufacturing process of ceramics, named hydrothermal-assisted transient jet fusion, pairing heat and pressure in attempts to create a highly dense green part. The process utilizes water as a transient binder to fuse particles eliminating the possible contamination caused by traditional organic binders. Inkjet printing was employed to selectively deposit water into a powder bed. Bentonite clay powder was used as a model material for the study, due to its excellent solubility in water. An analysis of the effects of pressure and heat on powder fusion was completed using the compression strength as a quantitative measure. A processing map was created to provide a preliminary understanding of the relationship between the combination of heat and pressure and selective fusion of powder. Test cases were printed to show the capabilities of the developed process. A prediction of the parts compressive strength was done based on previous data collected. Results proved that an increase in temperature culminates a higher compression strength. Results also showed that an increase in pressure contributes to a postponed evaporation of water in the part; once the evaporation has taken place, a denser part has a more dramatic increase in compressive strength.

Keywords: additive manufacturing; ceramics; jet fusion; bentonite; hydrothermal

1. Introduction

Ceramic additive manufacturing (AM) is a class of manufacturing processes that fabricate ceramic structures in a layer-by-layer fashion. The processes are capable of fabricating complex geometries extremely difficult to achieve via traditional machining processes. In ceramic AM, such as ceramic stereolithography and binder jetting processes [1], organic binders are typically utilized to bond ceramic particles together into a green part prior to further densify via furnace sintering. The introduction of high volume-fractions of binders inevitably contaminates the powder and the part with unwanted additives, which consequently leads to the significantly reduced density of the final part during the solidification process [1].

In this paper, we present a new AM process for ceramics, named hydrothermal-assisted transient jet fusion (HTJF), which utilizes water as a transient binder to fuse particles eliminating the high porosity caused by traditional organic binders. More specifically, the HTJF process selectively deposits water as a transient binder into a ceramic powder bed and applies a hydrothermal environment (i.e., low heat and low pressure) to the powder bed to fuse the particles together through a water-mediated dissolution-precipitation mechanism. The novelty of this paper is the inclusion of heat and pressure

10.1016/j.promfg.2020.05.116

within the printing process to assist hydrothermal fusion of the particles, which provides an alternative approach to bond ceramic particles into green parts as compared to conventional binder-based adhesive bonding approaches. Bentonite clay powder was chosen as a model material, due to its low cost and suitable water-solubility (i.e., partially dissoluble in water).

The aims of this paper are to assess the effects of an applied hydrothermal condition (including temperature and pressure) on the properties (shape fidelity and compression strength) of green parts created by the HTJF process. Our hypothesis is the compressive strength of bentonite clay parts fabricated by the HTJF process will be increased when subjected to an increase in pressure and heat, and the relationship will be a bell curve, where at a certain point, the mechanical properties will start to decrease as the temperature continues to increase.

2. Background

Additive manufacturing of ceramics has been a topic of interest for years. Complex ceramics can be achieved through a variation of processes including stereolithography (SLA) [2, 3], selective laser sintering (SLS)[4, 5], binder jetting (BJ)[6-8], etc. A key challenge associated with conventional ceramic AM processes lies in the required use of a high volume-fraction of organic binders in shaping green parts, which significantly restricts the final density of ceramics that can be achieved by those AM processes. For example, green parts fabricated by BJ may contain a high volume-fraction of binder (e.g., saturation level greater than 60% [1]), which led to a sintered density as low as 27% by weight. Other process such as SLA [2] uses photocurable polymers as binders. The polymers are cured using ultraviolet light, which requires a high volume-fraction of the polymers (e.g., 60vol%) in a ceramic slurry to ensure proper photocuring properties of the materials. The high volume-fractions of binders required in these processes inevitably introduce substantial porosity in place of the decomposed binders after binder pyrolysis, which may not be eliminated even after sintering.

Several attempts have been made to increase the relative density made by ceramic AM processes. Zocca et. al. [9] studied the effects of layer thickness in promoting the final density of ceramics using SLS. Findings showed layer thickness had a significant role on the relative density. A bell curve relationship was seen in deriving the optimum layer thickness for maximum relative density. Using a BJ process, another study [7] examined the effects of particle size and layer thickness on the relative density of green bodies. Results showed that with the smallest particle size and smaller layer thickness, a relative density reaching 96% might be achieved. In a similar fashion, for SLS [5], the smaller the particle size, the more dense a part can become as well. Alternatively, Kunchala and Kappagantula [10] examined the introduction of nanoparticle densifiers in printing binders to enhance the mechanical performance of ceramics made using BJ. Although the nanoparticles increased density to some extent, the density is restricted by the low solids loading of nanoparticles in the binder that can be printed in the BJ process. While the improvement achieved by mentioned approaches was notable, the resulting density was still considerably less than that achieved by traditional ceramic manufacturing methods (e.g., over 98%).

3. Methods

3.1 The Fabrication Process

In this paper, we present a hydrothermal-assisted transient jet fusion process for achieving high green density of ceramics containing no organic binder. Inspired by the lithification process in rock formation[8], the HTJF process selectively deposits water into a powder bed of ceramic nanoparticles in a similar manner as binder jetting and subsequently applies a low heating temperature (e.g., 50-200^{o}C) and a high uniaxial pressure (e.g., 0-14500PSI) to the whole powder bed, enabling a hydrothermal environment in the powder that fuses the water-saturated nanoparticles together while keeps dry particles remain loose. Since the deposited water completely evaporates out of the powder compact, the obtained green part contains no binder between nanoparticles. For more details about the fusion mechanisms involved in the HTJF process, interested readers may refer to our prior work [8].

The HTJF system is primarily comprised of an electrically controlled uniaxial press, a powder bed, and an inkjet printing platform, as shown in Fig.1 and Fig. 2. The uniaxial press is capable of applying high pressures (up to 14500PSI) onto the powder bed through a pressing piston, which is driven along a guide by a high torque Nema 34 stepper motor connecting to a high ratio gearbox and a leadscrew. The press was assembled on a high strength H-frame dissected from a commercial 12-ton hydraulic press to ensure maximum rigidity during pressing. Fig. 1a shows positioning of the uniaxial press prior to pressing, and Fig. 1b shows positioning during pressing. In a similar fashion to the piston in the uniaxial press, the powder bed was connected to a linear screw which was then attached to a motor. A load cell was placed under the powder bed to measure the pressure applied by the top pressing piston.

Between the press and the powder bed, an inkjet printing platform was mounted. An inkjet printhead was dissected from a commercial Canon inkjet printer and modified with a refillable cartridge. The printhead was fixed on a one-axis slide and connected to a belt and pulley mechanism to allow for movement perpendicular to the printhead's axis. A roller was connected to the same axis to spread the powder from the powder storage. Fig. 2 demonstrates the powder bed and powder movement throughout the printing process. Fig. 2 a. shows the printer prior to printing and Fig. 2 b. shows the printer after printing.

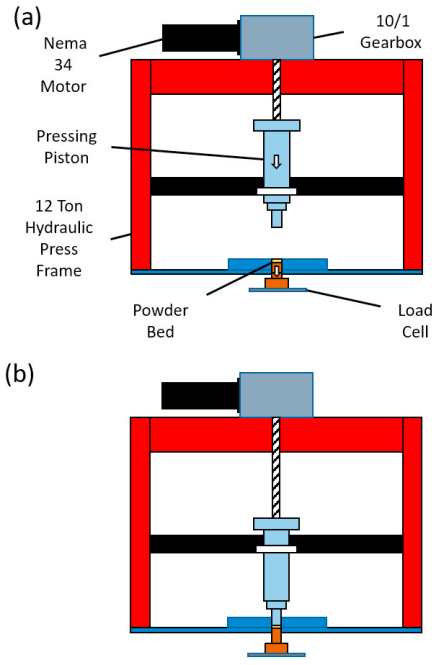

Fig. 1 The electrically controlled uniaxial press subsystem: (a) Prior to press; (b) Pressing

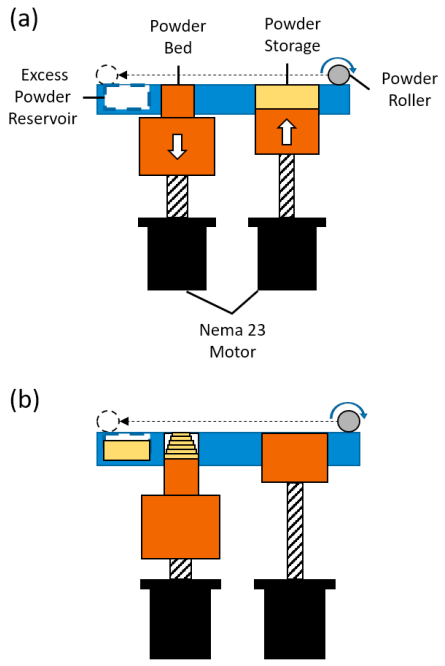

Fig. 2 The inkjet printing subsystem: (a) Prior to print; (b) After print

3.2 Printability testing

In the present work, water was used as a printing binder, and bentonite clay powder (Bulk Apothecary, Ohio, USA) was selected a model material for testing the process due to its excellent solubility in water. Printability of the bentonite clay via the proposed HTJF process came with several visible issues. The first issue uncovered was curling of a powder layer when exposed to water. The exterior of the printed layer immediately curled which interfered with the printer head, often destroying the part or diminishing the part quality. The second issue involved cracking of the printed part when exposed to heat, preventing fabrication of a whole part. The third issue involved separation between the printed layers. For successful printing, these issues had to be solved. To solve the curling, each layer required flattening of the curled edges with a blade. To eliminate the cracking, the water distribution was adjusted along with the rate of curing. To fix the layer separation, the water distribution was optimized. Further details are provided in the results section.

3.3 Investigation on the effects of temperature/pressure

Once a part was printed, qualitative and quantitative tests were performed on the part to evaluate the strength of particle fusion. In qualitative tests, visual observations were used to deduce if the part was tacky or solidified. A solid part had a much brighter color when compared with a tacky part. Observations were also made to see how strong the part was. Strength of the part was observed by pressing the part between fingers. A weak part would crumble back into its original powder form, while a strong part held its shape when pressed between fingers. The part was also prodded with a needle to determine the boundary strength of the part. The boundary for the printed part could be seen in the dry powder, so the needle would scrape the edges to break away the loose powder. A solid part kept a fine boundary without breaking when subjected to scraping.

Quantitative tests were used to determine the mechanical properties of the printed part. Compression tests were performed with a Test Resources compression test machine to quantify the parts compression strength. The machine paired with a Newton software for control. The machine used a maximum force of 999lbs while performing a compression test. The part was placed in the tester, and the software initialized the compression test. Once the tester reached 999lbs, the Newton software gave the results for the test. The software provided the stress and strain and specific points in time during the test. With the stress and strain, the compressive strength was compared by looking at the stress value at selected strain points.

For testing of pressure and temperature, pre-mix parts were used. The parts were made at 30wt% water and 70wt% bentonite powder. The water and powder were placed on a scale to determine the weight, and once the correct amount was given for the corresponding weight percentage, the combination was mixed with a steel prod. The material was mixed until the dry

powder could no longer be seen. The pre-mixed material was placed in a 20mm diameter circular mold, at 1mm thick. Pre-mixed material was used rather than printed parts to speed up the testing process. The pre-mixed parts were then placed in a stainless-steel die as shown in Fig. 3.

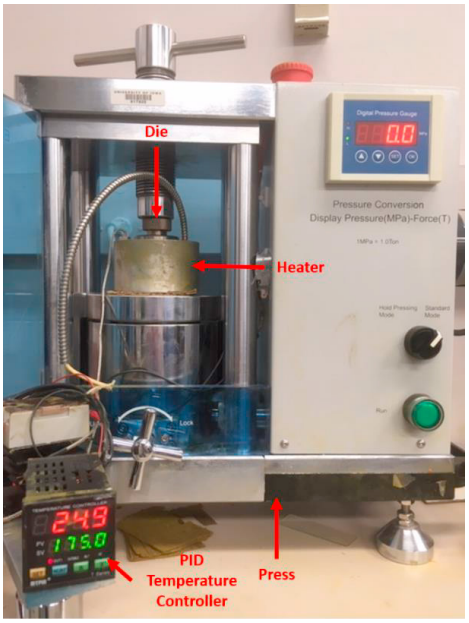

Fig. 3 A testing system consisting of a die, press, and heater

To adjust the pressure, the die was placed in an 30T desktop electric hydraulic laboratory press. The press applied a force on the die at 2PSI, 870PSI, and 7252PSI. To adjust the heat, the die was placed in a PID temperature-controlled heater. The PID temperature controller was adjusted to 75ºC, 100ºC, 125ºC, 150ºC, and 175ºC. All subjects were exposed to the heat and pressure for 10 minutes. The repeatability of the testing results was checked by performing additional runs for selected samples. Similar repeatability checking has been used in prior studies on ceramic sintering [11]. Based on the results, an understanding of mechanical properties of the part with respects to varying pressure and temperature combinations was gained. Optimum parameters were selected from the results, which were then applied towards a printed part.

3.4 Testcase fabrication

For a printed part, the desired shape was created in a word document. The part was printed on a 20mm diameter aluminum tab to ease the removal from the powder bed. Prior to the start of printing, a light layer of glue was applied to the tab using a glue stick to ease the attaching of the base layer to the tab. An Arduino code was created to spread a layer of powder at the desired layer depth. Using the Nema 23 motors, the Arduino code raised the powder storage while lowering the powder bed. The roller transported the powder from the powder storage to the powder bed. In this case, the layer depth was .228 mm. Once the layer was spread, the word document was uploaded to the inkjet printer which contained water rather than ink. The inkjet printer then deposited the water in the desired pattern onto the powder bed. In the event of layer curling, a knife blade was used to lightly flatten the curled edges. Another layer was then spread, and the process repeated. Once the part reached 5 layers, the part was removed from the printer on the aluminum tab. The printed part was placed in the die to proceed with testing.

3.5 Processing map

A preliminary understanding of the relationship between the combination of heat and pressure and selective fusion of powder was required. To do so, a processing map was created. Parts were printed under varying parameters and then observed to see if the part was still tacky or solid. The temperature was adjusted from 110ºC to 150ºC with increments of 5ºC being tested. The time of heating ranged from 30 seconds to 10 minutes. To determine the part's strength, the color of the part was examined. A tacky part had a dark color, while a solid part had a lighter color. Some parts had solid edges but tacky centers. These parts were considered the boundary line for the transition point. Based on the results, a processing map was created to enable the selection and optimization of process parameters for the HTJF process.

4. Results and Discussion

4.1 Prototype machine

Figure 4 shows a prototype machine for the proposed HTJF process. A Nema 34 motor with 1841 oz/in was paired with a 10/1 right angled gearbox. The gearbox was connected to a 3/4" thick precision lead screw. A precision nut made for the lead screw was threaded onto the lead screw and attached to a piston made from .25" walled 1.5" diameter pipe. The pipe had a 20mm tip fastened into which served as the end of the press. To prevent rotation, the nut was fixed onto a plate. The plate had holes drilled in both ends with bearings placed inside. 1/8" rods were fed through the bearings and the ends were fixed onto the frame of the press. Therefore, when the motor was turned on, the gearbox would rotate the leadscrew. With the nut not being able to rotate, the nut would move the piston up and down depending upon the direction of motor rotation. Calculations were done to determine the maximum pressure the machine was capable of. Based on the torque of the motor, the gearbox, and a few assumed variables, the machine can apply a maximum pressure of 14,500 PSI.

The powder bed was constructed in the same fashion as the press but replaced the motor with a Nema 23 motor and removal of the gearbox. The lead screw was 5/8" rather than 3/4". A load cell was placed under the powder bed to determine the amount of pressure applied by the press on the powder bed. The powder storage also used a Nema 23 motor with a 3/8" lead

screw. An aluminum cylinder was fixed onto the end of the lead screw.

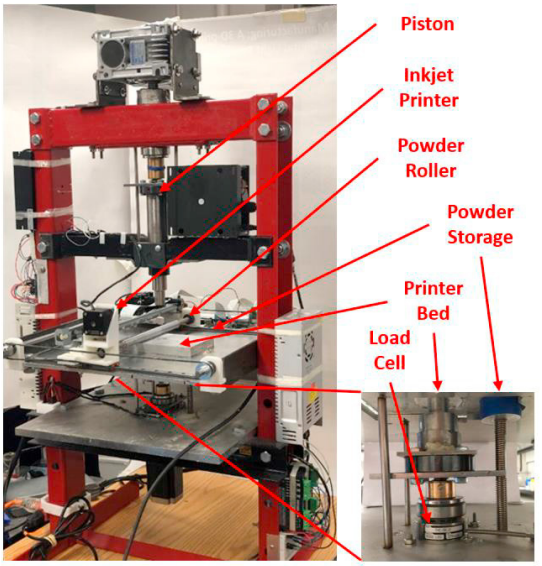

Fig. 4 A prototype machine for the proposed HTJF process

4.2 Curling

Curling was noticed during early layers of printing. Prior studies have reported similar phenomenon. Kodicara and Kappagantula [12] examined the curling of bentonite during desiccation. They found an increase in moisture content as well as a longer duration drying time induced the curling of a sintered part. This was believed to be induced by differential shrinkage strain increments. Fig. 5 illustrates the curling mechanism. The printer deposits water onto the powder bed. Evaporation of the water begins to take place, but only at the upper, exposed, levels of the part. The evaporation causes shrinkage in the part in the upper layers. As the shrinkage of the top layers takes place, the differential shrinkage strain begins. Due to the strain brought on by differential shrinkage, the top layer edges begin to curl upward.

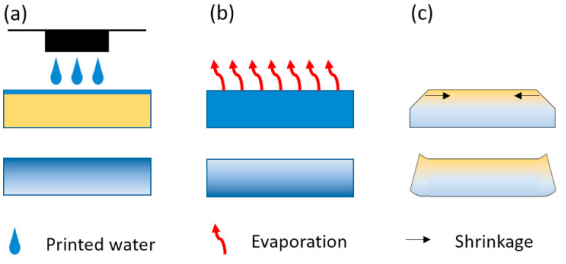

Fig. 5 (a) Water deposited; (b) Evaporation takes place; (c) Differential shrinkage

To solve the issue, a glue stick was applied to the printer bed. Then, after the first two layers were printed, they were lightly pressed to help the powder stick to the base. Top layers were able to adhere to the layers below preventing curling errors. Fig. 6 shows the print prior to light pressing and after pressing. The edges have adhered to the bed keeping the curling from persisting.

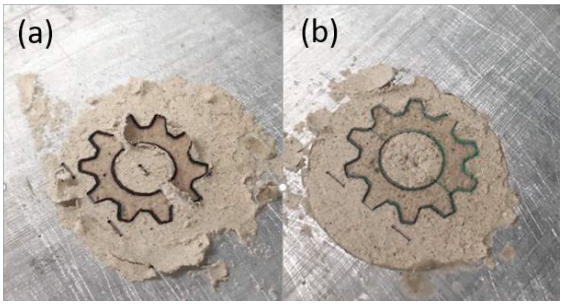

Fig. 6 (a) Before light pressing; (b) after light pressing

An alternative that has been tested to resolve the issue was through controlling the humidity of the printing environment. With desiccation being the initiating agent, the evaporation would be the main cause. Higher evaporation rates often ensue in dryer environments. To test the effect of humidity on the print, the printer bed was enclosed with plastic films. A small household humidifier was placed inside the enclosure along with a humidity gauge. A small fan was place on the edge of the plastic. With this setup, the humidifier could be turned on until the humidity reached the desired level. The fan could be turned on if the humidity level was too high. At the desired humidity level, the print would take place. *Table 1* displays the results of the trials.

Table 1. Humidity trial results

Humidity Level	Rolling of Powder	Curling	Comments
64%	Light stick on roller	Moderate	3 print passes
68%	Light stick on roller	Limited	Restarted humidifier
68%	Light stick on roller	Moderate	3 print passes
69%	Light stick on roller	Moderate	3 print passes
69%	Light stick on roller	Moderate	3 print passes
70%	Stuck on roller	-	Part stuck to roller
70%	Light stick on roller	Moderate	3 print passes
70%	Light stick on roller	Moderate	6 print passes
75%	Light stick on roller	Moderate	6 print passes
75%	Light stick on roller	Moderate	3 print passes
80%	Light stick on roller	Moderate	6 print passes
80%	Light stick on roller	Moderate	6 print passes
84%	Light stick on roller	Minimal	6 print passes, damp powder bed
84%	Light stick on roller	Moderate	6 print passes
85%	Light stick on roller	Minimal	6 print passes, damp powder bed
85%	Light stick on roller	Moderate	6 print passes

An increase in humidity resolved the curling issue at around 84% humidity. A problem arising from the increased humidity was the powder outside the printed area became too saturated causing the powder particles to adhere to one another. The printed area and the powder surrounding couldn't be separated as desired. The saturated area also prevented the spreading of the powder using the roller. Once damp, the powder would stick to the roller rather than spread out evenly, therefore, concluding the testing of humidity for the method wasn't suitable for the application

4.3 Cracking

Cracking was another issue during the printing process. Prior research papers extensively studied the causes for the cracking of clay during drying. Lloret et. al. [13] looked at the void ratio, another way to understand density, under increasing pressure. Lloret [13] found the void ratio decreased as the pressure increased. A smaller void ratio would relate to a denser part. With a denser part, one could expect a smaller void ratio which reduced the amount of cracking. Other studies involving bentonite have been focused on the swelling and curling nature of the material. Bronswijk [14] found with an increase in moisture content, the void ratio of the powder increases. Again, a greater void ratio was induced by the swelling of the material due to higher amounts of moisture. This could be expected with bentonite being quite soluble in water. Additionally, Bronswijk [14] found the shrinkage while drying increases with the increase in moisture. The more a part shrinks, the more the cracks will appear. Tariq [15] confirmed those results with similar studies finding a larger content of moisture leads to more cracking within the clay. Swelling and shrinkage of most solid objects often cause cracking, and bentonite is of no difference. With the adjustment of certain parameters, cracking of the final part was reduced or eliminated.

As the studies suggested, the amount of water had a clear effect on the cracking. With less water, less cracking occurred. 4 weight percentages of water were mixed in the same fashion as the pre-mixed material for testing. The weight percentages were 22%, 34%, 46%, and 60%. The first 3 percentages were derived from the amount of water of 3, 6, and 9 printing passes by the inkjet printer. The values were found by printing 3, 6, and 9 passes using the word document. If a shape was on the word document 3 times, the printer would pass by 3 times. If on the document 6 times, the printer would pass 6 times. The water was printed onto a tab, and the tab was weighed with and without the water. The difference was the weight of the water with specified printing passes. 60% was an extreme case for further testing. The 22% weight water part had no visible cracking. The 60% water part had very significant cracking. Fig. 7 shows the testing results.

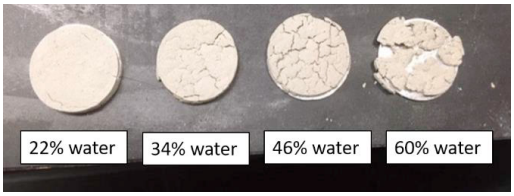

Fig. 7 Cracking with water percentage adjustments

4.4 Effects of temperature on compression strength

The increase in temperature showed a significant improvement in compression strength. Fig. 8 demonstrates the process in which particles are hydrothermally bonded. The water is deposited onto the powder bed. With the bentonite having a high solubility in water, the introduction of water repositions and reshapes the powder particles. The soluble surfaces of the particles come in contact with one another, resulting in stress-assisted dissolution at the contact points. As the water evaporates, the dissolved species are redistributed by the capillary flow and precipitate at the contact points, thus bonding the particles into one solid part. The schematic of the microstructure evolution from the beginning to end shows how the particles are bonded when the part is exposed to water and heat. Particles in the beginning are large and separated but the end shows much tighter particles allowing for improved strength.

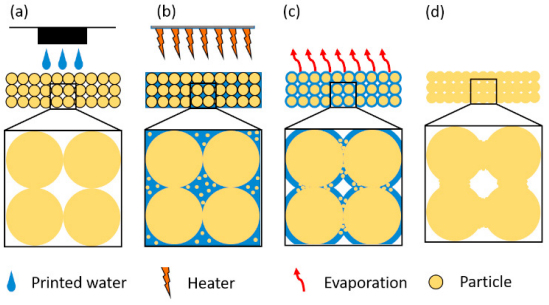

Fig. 8 (a.) Water deposited; (b) Heater evaporates water; (c) Particles bond

Fig. 9 quantifies the effects of temperature on compression strength. It shows steadily increasing trends in yield strength (i.e., 10%, 15%, and 20% yield) as temperature increases. The black lines represent a clay powder without any water, which serves as a baseline for comparison. The dry powder had a greater or equal compressive strength until the temperature became high enough for the water to evaporate out of the part, which is represented by the intersection of the black line with the other lines. The dry powder has a greater compressive strength due to the substantial packing density compared to the wet, tacky clay.

Fig.9a represents the temperature-strength relationships under a constant pressure (10 minutes) of 2PSI. When the

temperature was lower than 100ºC, the compressive strengths were relatively stable. After the temperature increased above 100ºC, the water started to evaporate, and the compressive strength dramatically increased. The evaporation of the water allows particle bonding within the part, and therefore, strengthening the part. In Fig.9a, the transition starts around 100ºC. In Fig. 9b, the pressure is increased to 870PSI. With a greater pressure, the stability is prolonged, and the transition point starts at around 125ºC. The greater pressure increases the density of the part, and a denser part hinders the evaporation process. Fig. 9c shows a steeper pressure, again, extending the transition point to a later temperature. With 7252PSI, the transition point is around 150ºC.

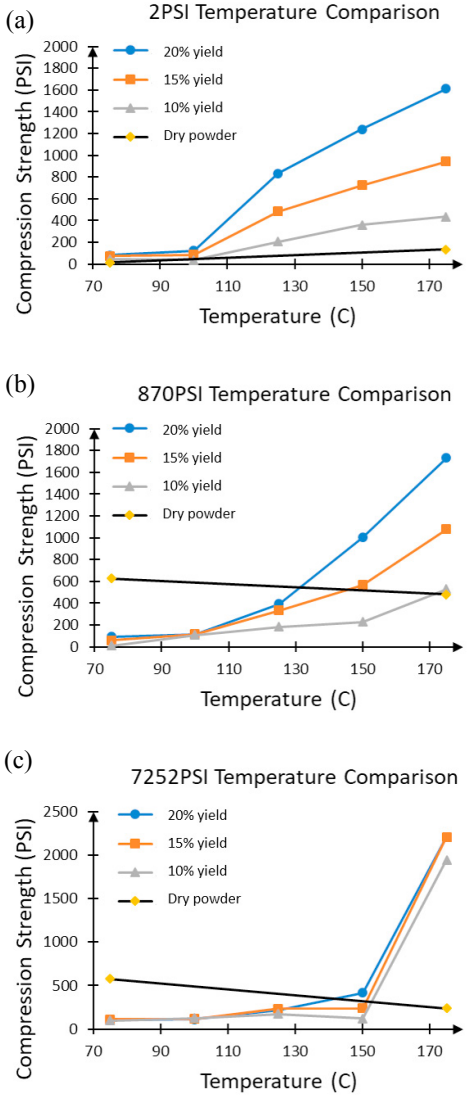

Fig. 9 Compression strength at (a) 2PSI; (b) 870PSI; (c) 7252PSI

A comparison of this noticeable difference where the point transitions from stable to an increasing trend can be seen in Fig. 10. Clearly, the higher the pressure, the higher the temperature needs to be for the transition to take place. Fig. 11 demonstrates the evaporation of water when pressure is changed. The pores within the part creates capillaries for the water to escape. The smaller the pores, the smaller the capillaries allowing less water to escape. The 2PSI part has a lower density which creates larger pores and capillaries. This allows for water to escape and evaporate easier from the part. As the pressure increases, the pore size decreases along with the capillaries, which slows the rate of evaporation. Therefore, it takes a higher temperature to penetrate the part to evaporate the water, as Fig. 10 shows.

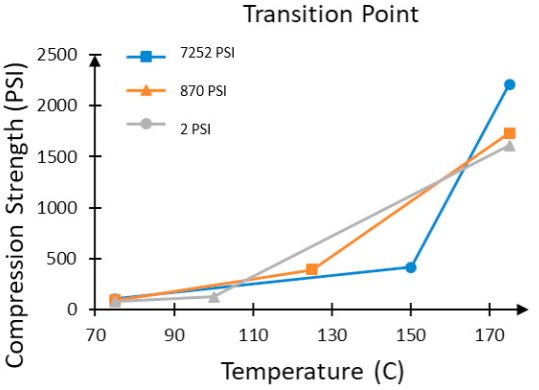

Fig. 10 Transition point

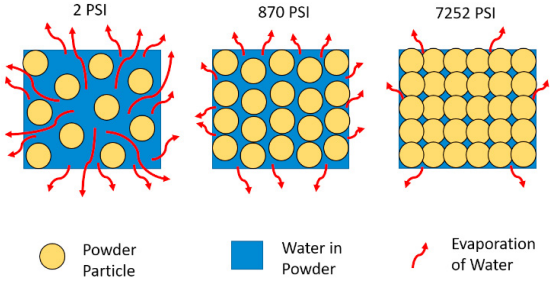

Fig. 11 Water evaporation with respects to pressure

Similarly, the rate of increase for compressive strength was greater for higher pressures. Fig. 12 shows the increasing slope of compression strength after the transition point under different pressures. With a higher pressure causing the evaporation taking place at a later point for the part, the temperature which the part was exposed to was much greater. A higher temperature causes a higher rate of evaporation, which causes the greater increasing rate in the compressive strength.

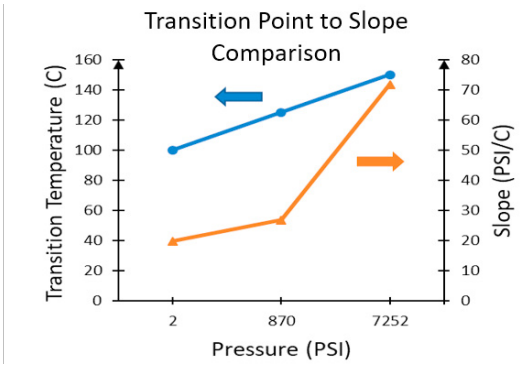

Fig. 12 Slope after transition point

4.5 Effects of pressure on compression strength

Fig. 13 represents the differentiation in compressive strength under different pressures at a given temperature ranging from 75ºC to 175ºC. All data gathered was at 20% yield strength. Three pressures were tested, including 2PSI, 870PSI, 7252PSI. The results showed very little change at the lower temperature. This was expected for the evaporation of water has yet to take place in any of the three pressures. A slight increase was seen at 100ºC. Again, the evaporation has yet to take place in the higher pressure, but just starts initiating at 2PSI. At 125ºC, one can see the evaporation has a great effect on the lowest pressure and starts to take place in the 870PSI test. As mentioned before, as the water evaporates out of the part, the compressive strength increases due to particle bonding. At 150ºC, the compressive strength has dramatically increased for both 2PSI and 870PSI. The 7252PSI test showed the evaporation has started taking place. At the highest temperature 175ºC, a dramatic increase can be seen in all 3 pressures. The data collected for pressure comparison aligned with that of the temperature comparison. The transition points from stable to an increasing trend were seen under the same conditions, where evaporation of the water started taking place.

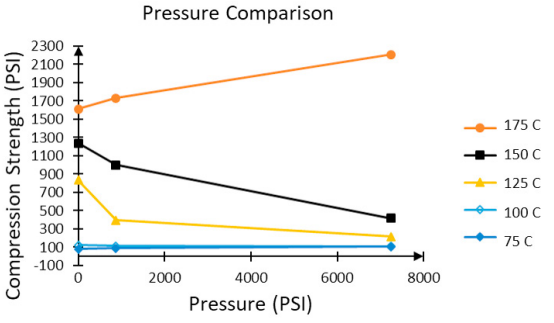

Fig. 13 Pressure comparison at different temperatures

4.6 Processing map

Fig. 14 shows the processing map created for preliminary understanding of the parameter space for selectively fusing clay particles. The comparison of temperature with respects to time showed a trend which was mapped. For example, a sample at 125ºC for 6 minutes proved to be a solid part. The process parameters leading to a solid part were labeled as a circle in the map. A sample was taken at 115ºC for 8 minutes had solid edges but a tacky center. This proved to be the transition point between tacky and solid and received a line segment for mapping. A sample taken at 110ºC for 7 minutes proved to be tacky and was mapped as an x. The process continued until the boundary was found, as shown in Fig. 14. The light blue area is a transition region when one can expect the part to become solid under specific time and temperatures. The relationship was quadratic as the figure shows. As the temperature increases, the time to solidify decreases.

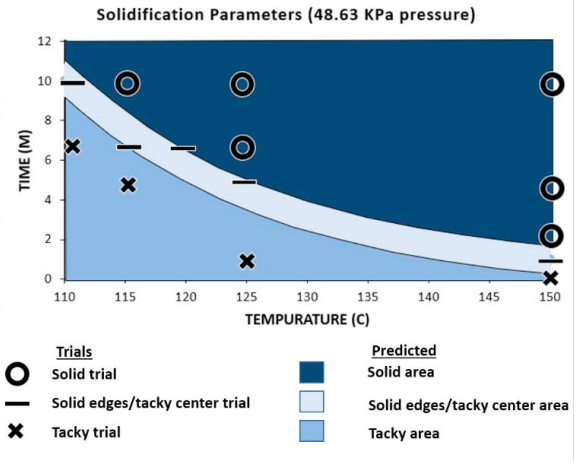

Fig. 14 Processing Map

4.7 Test cases

The results from the pre-mixed parts were used to predict the compressive strength of a printed part based on the temperature at a specific pressure. To do so, a compression test of 2 printed parts was performed. The printed part was a circle which resembled the shape of die, used for the pre-mixed parts. The results were compared with the results of the pre-mixed trials. The optimum parameters for a printed part was found at 2PSI, so this pressure was chosen for the printed parts. This was the optimum pressure for the part was strong and had little diffusion of the water. Higher pressures diffused the water and the shape which was printed came out distorted. Fig. 15 shows the printed parts (gold color) and the pre-mixed parts (blue color). The lines represent 10%, 15%, and 20% yield strength. The trials for the printed parts were done at 125ºC and 175ºC to capture the slope after the transition point. The pre-mixed parts had a higher compressive strength because the water was more evenly distributed. With the pre-mixed parts, the water was forced into the powder with the prod. Pressure and

manipulation of the powder allowed for uniform distribution. The printed parts had water deposited onto them, so the water was evenly distributed in the X and Y direction, but the distribution was less adequate in the Z direction causing weaker parts when compared with the Pre-mixed parts. The two parts, however, had the same increasing trend. As the temperature increased, so did the compressive strength. The printed results and pre-mixed trials were paired to predict the compression strength of the other data points for temperature. Fig. 16 shows the prediction using a data driven method, based on a procedure by Rasmussen [16]. The figure has a 95% confidence interval to account for error.

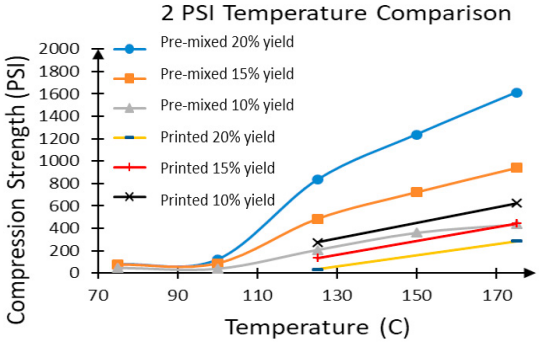

Fig. 15 Printed and pre-mixed comparison

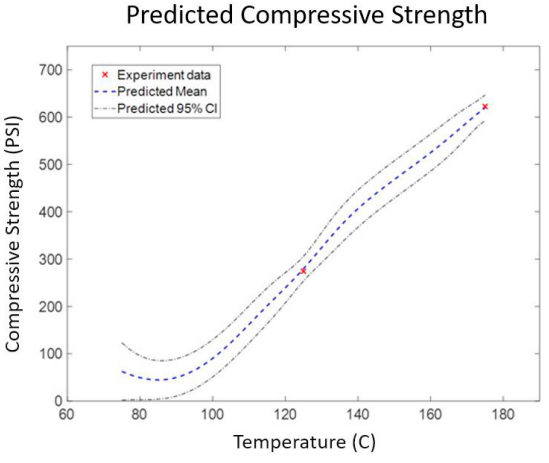

Fig. 16 Printed part prediction

The capabilities of the printer are just beginning to be explored. Fig. 17 shows examples of test cases which have been printed by the HTJF process. Fig. 17a shows the original shapes which were imported into the printer. Fig.17b is a solid gear showing the top and lateral view. The thickness of the part is 3mm and was printed with 15 layers. Fig. 17c shows a panda which was printed showing the complexity of the HTJF process. An outline was printed with water (First picture in Fig. 17a). 15 layers were printed at a total thickness of 3mm. Ink was then printed on top to show the multi-material capabilities of the printer using the second image in Fig. 17a. 2.5D objects have been fabricated, however, future studies will investigate true 3D shape printing capabilities as full automation is implemented.

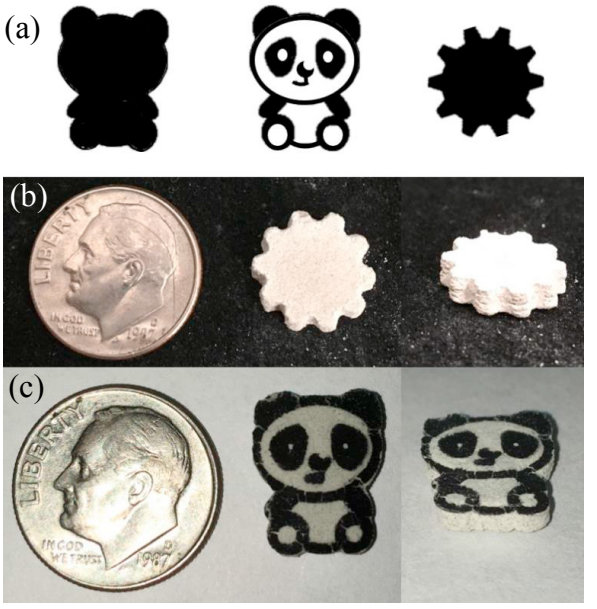

Fig. 17 Test cases via the HTJF process

5. Conclusion

The present study allowed for development of a new AM process which introduces hydrothermal conditioning to a binder jetting process. The combination of a pressing mechanism within a 3D printer was achieved. Additionally, the HTJF process eliminated the use of binders through substitution of water. Contamination of the powder bed was eradicated with the introduction of water. Multiple problems were encountered within the printing of bentonite clay powder. With the issue of curling of the printed part, a method was devised to allow printing through flattening of the curled edges. A method to account for cracking was brought forth involving reduction in water percentage. Testing of pre-mixed material proved an introduction of thermal conditioning has a dramatic effect on the compressive strength. The point at which the compressive strength increases varies depending upon the pressure applied to the part. The greater the pressure applied, the slower the evaporation rate of the part causing a slower rate of increase in compressive strength. Once the transition point has occurred, the rate of compression strength has a greater slope in the

compacted part for the temperature is much higher at this point. Aside from analysis, the data was used to predict the compressive strength of a printed part preventing an abundance of time and effort brought forth by printing. With the method used, pre-mixed parts could be used to determine the optimum conditions for a printed part rather than printing and testing numerous parts.

Acknowledgement

The authors acknowledge the funding support from the Iowa Technology Institute for this research.

References

[1] Gaytan, S. M., Cadena, M., Aldaz, M., Herderick, E., Medina, F., and Wicker, R., 2013, "Analysis of ferroelectric ceramic fabricated by binder jetting technology," Proceedings of Solid Freeform Fabrication Symposium, pp. 859-868.

[2] Griffith, M. L., and Halloran, J. W., 1996, "Freeform fabrication of ceramics via stereolithography."

[3] He, L., Fei, F., Wang, W., Song, X. J. A. a. m., and interfaces, 2019, "Support-Free Ceramic Stereolithography of Complex Overhanging Structures Based on an Elasto-viscoplastic Suspension Feedstock," 11(20), pp. 18849-18857.

[4] Kruth, J. P., Mercelis, P., Van Vaerenbergh, J., Froyen, L., and Rombouts, M. J. R. p. j., 2005, "Binding mechanisms in selective laser sintering and selective laser melting."

[5] Sing, S. L., Yeong, W. Y., Wiria, F. E., Tay, B. Y., Zhao, Z., Zhao, L., Tian, Z., and Yang, S. J. R. P. J., 2017, "Direct selective laser sintering and melting of ceramics: a review."

[6] Manogharan, G., Kioko, M., and Linkous, C. J. J., 2015, "Binder jetting: a novel solid oxide fuel-cell fabrication process and evaluation," 67(3), pp. 660-667.

[7] Gonzalez, J., Mireles, J., Lin, Y., and Wicker, R. B. J. C. I., 2016, "Characterization of ceramic components fabricated using binder jetting additive manufacturing technology," 42(9), pp. 10559-10564.

[8] Fei, F., He, L., Zhou, B., Xu, Z., and Song, X., in press, "Hydrothermal-assisted Transient Binder Jetting of Ceramics for Achieving High Green Density," JOM.

[9] Zocca, A., Gomes, C. M., Bernardo, E., Müller, R., Günster, J., and Colombo, P. J. J. o. t. E. C. S., 2013, "LAS glass–ceramic scaffolds by three-dimensional printing," 33(9), pp. 1525-1533.

[10] Kunchala, P., Kappagantula, K. J. M., and Design, 2018, "3D printing high density ceramics using binder jetting with nanoparticle densifiers," 155, pp. 443-450.

[11] Rahaman, M. N., De Jonghe, L. C., and Chu, M. Y. J. J. o. t. A. C. S., 1991, "Effect of green density on densification and creep during sintering," 74(3), pp. 514-519.

[12] Kodikara, J. K., Nahlawi, H., and Bouazza, A. J. C. G. J., 2004, "Modelling of curling in desiccating clay," 41(3), pp. 560-566.

[13] Lloret Morancho, A., Villar, M. V., Sanchez, M., Gens Solé, A., Pintado Llurba, X., and Alonso Pérez de Agreda, E., 2003, "Mechanical behaviour of heavily compacted bentonite under high suction changes."

[14] Bronswijk, J. J. B. J. J. o. H., 1988, "Modeling of water balance, cracking and subsidence of clay soils," 97(3-4), pp. 199-212.

[15] Tariq, A.-u.-R., and Durnford, D. S. J. S. S. S. o. A. J., 1993, "Analytical volume change model for swelling clay soils," 57(5), pp. 1183-1187.

[16] Rasmussen, C. E., 2003, "Gaussian processes in machine learning," Summer School on Machine Learning, Springer, pp. 63-71.